NANO LETTERS

Letter

pubs.acs.org/NanoLett

# Gate-Defined One-Dimensional Channel and Broken Symmetry States in $MoS_2$ van der Waals Heterostructures

Riccardo Pisoni,[†] Yongjin Lee,[†] Hiske Overweg,[†] Marius Eich,[†] Pauline Simonet,[†] Kenji Watanabe,[‡] Takashi Taniguchi,[‡] Roman Gorbachev,[§] Thomas Ihn,[†] and Klaus Ensslin*,[†]

[†]Solid State Physics Laboratory, ETH Zürich, CH-8093 Zürich, Switzerland

[‡]National Institute for Material Science, 1-1 Namiki, Tsukuba 305-0044, Japan

[§]National Graphene Institute, University of Manchester, Manchester M13 9PL, United Kingdom

**ABSTRACT:** We have realized encapsulated trilayer $MoS_2$ devices with gated graphene contacts. In the bulk, we observe an electron mobility as high as 7000 $cm^2/(V\ s)$ at a density of $3 \times 10^{12}$ $cm^{-2}$ at a temperature of 1.9 K. Shubnikov–de Haas oscillations start at magnetic fields as low as 0.9 T. The observed 3-fold Landau level degeneracy can be understood based on the valley Zeeman effect. Negatively biased split gate electrodes allow us to form a channel that can be completely pinched off for sufficiently large gate voltages. The measured conductance displays plateau-like features.

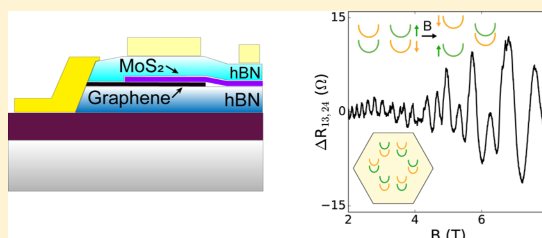


**KEYWORDS:** *$MoS_2$, van der Waals heterostructures, Shubnikov–de Haas oscillations, valley Zeeman effect, gate-defined nanostructures*

Laterally confined two-dimensional (2D) materials offer the opportunity to engineer quantum states with tunable spin, charge, and even valley degrees of freedom.[1−3] The pure thinness of these materials in combination with 2D insulators such as boron nitride pave the way for ultrasmall strongly coupled gate-defined quantum devices.[4−7] In addition, the variety of transition metal dichalcogenides (TMDCs) materials will allow one to choose a different strength of spin–orbit interaction that is relevant for electric control of spin and valley states in view of quantum information processing. In this Letter, we describe a split gate geometry realized on a high-quality molybdenum disulfide ($MoS_2$) van der Waals heterostructure that results in a tunable tunneling barrier, the starting point for any electronic quantum device. The electronic quality of our trilayer $MoS_2$ device is documented by the observation of Shubnikov–de Haas oscillations (SdHO) occurring at magnetic fields as low as 0.9 T. In addition a 3-fold degeneracy of the Landau levels (LLs) is observed arising from the 3 Q and 3 Q′ valleys situated in the middle of the Brillouin zone and shifted in magnetic field by the valley Zeeman effect.[8−12] The constriction can be completely pinched off with resistances values exceeding the quantum of resistance $h/e^2$ by orders of magnitude, a prerequisite for the realization of any single-electron transistor. We observe the occurrence of plateau-like features in the conductance with a spacing of the order of $e^2/h$. These experiments are a first step toward gate-controlled quantum devices in transition metal dichalcogenides.

**Results and Discussion.** To achieve high mobility TMDC devices, we fabricate $MoS_2$-based van der Waals heterostructures. As shown schematically in Figure 1a, a trilayer $MoS_2$ flake (~2 nm thick), contacted with two few-layer graphene (FLG) sheets, is encapsulated between hexagonal

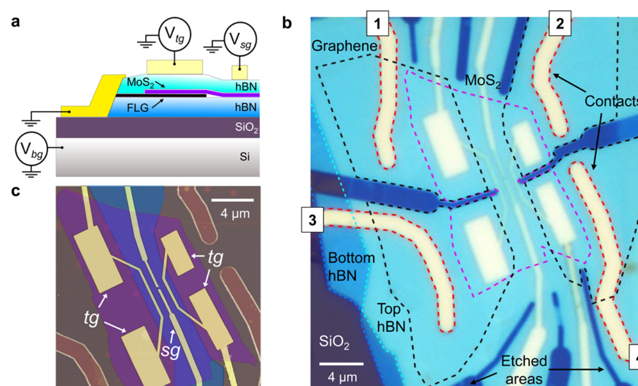


**Figure 1.** (a) Cross-sectional schematic of the $MoS_2$-based field-effect device. (b) Optical micrograph of the device. An encapsulated trilayer $MoS_2$ (purple dashed lines) is connected to two graphene flakes (black dashed lines). Au/Cr one-dimensional edge contacts (numbered 1−4) to the graphene flakes are fabricated.[17] The dark blue regions outline the etched areas that define the final device geometry. (c) False-color AFM image of the device before the last etching process. Four rectangular gates have been deposited on top of the contact areas between graphene and $MoS_2$ in order to reduce the contact resistance without affecting the low carrier density in the $MoS_2$ channel. A split gate, defining a nanoconstriction, has been placed on top of a bubble-free region.

boron nitride (hBN) crystals.[13−15] The bottom one is 30 nm thick and separates the $MoS_2$ from substrate phonons and

Received: May 24, 2017
Revised: June 28, 2017
Published: July 7, 2017

 © 2017 American Chemical Society 

DOI: 10.1021/acs.nanolett.7b02186
Nano Lett. 2017, 17, 5008−5011

charged impurities, further serving as an atomically flat substrate.[16] The top one is 20 nm thick and prevents the adsorption of organic residues during the fabrication process. To assemble the heterostructure we employ a polymer-based dry pick-up and transfer technique[17,18] using a polycarbonate film[19,20] supported by polydimethylsiloxane. Assembling and exfoliating the various thin films was performed in an argon environment.[21] The films' thicknesses were first determined from the optical contrast and then verified by atomic force microscopy (AFM). The top hBN crystal serves as the dielectric layer for the top gates whereas the $SiO_2$/n-Si substrate works as the bottom dielectric (285 nm) and gate electrode. The top gate structure consists of two pairs of local gates on top of the contact areas between graphene and $MoS_2$ and a split gate with a 100 nm gap (Figure 1c). In order to avoid electrostatic inhomogeneities, the split gate has been deposited on a bubble-free area on top of the $MoS_2$ channel, found by AFM. Cr/Au electrodes are used as one-dimensional edge contacts to graphene (red dashed lines in Figure 1b).[17] Finally, the four-terminal device geometry is defined by etching through the top hBN, $MoS_2$, and FLG (Figure 1b). As shown in Figure 1a, we can tune the carrier density in the $MoS_2$ channel by biasing the Si gate electrode ($V_{bg}$). We can further tune locally the carrier density in the contact area between $MoS_2$ and graphene ($V_{tg}$) and deplete the $MoS_2$ two-dimensional electron gas (2DEG) ($V_{sg}$).

Figure 2a shows the low temperature ($T$ = 4 K) two-terminal resistance as a function of $V_{tg}$, for different $V_{bg}$. The resistance decreases with increasing $V_{bg}$, as expected for an n-type semiconductor.[14] At fixed $V_{bg}$, the resistance drops for increasing $V_{tg}$ by up to 2 orders of magnitude. Figure 2b displays the estimated contact resistance $R_c = \frac{1}{2}(R_{12,12} - R_{12,34})$, where $R_{12,12}$ is the two-probe resistance and $R_{12,34}$ is the four-probe resistance of $MoS_2$ (Figure 1b). $R_c$ can be improved by up to 3 orders of magnitude with increasing $V_{tg}$. Figure 2c,d shows the current flowing into the device ($I$) as a function of the voltage applied between two graphene electrodes ($V_{bias}$). When $V_{tg}$ = 0 V, nonlinear $I-V_{bias}$ curves are observed indicating gapped-behavior corresponding to nonohmic contacts (Figure 2d). Linear behavior is achieved at higher $V_{bg}$ as already demonstrated in previous works.[13−15] We observe linear $I-V_{bias}$ curves at any $V_{bg} \geq 0$ V when $V_{tg} > 3$ V (Figure 2b). Therefore, we can locally tune the carrier density in the $MoS_2$ layer and the Fermi level of graphene to achieve ohmic contact without compromising the low carrier density in the $MoS_2$ channel. This allows us to investigate the physics of $MoS_2$ at the edge of the conduction band.

To examine the quality of our device we performed magnetotransport measurements at $T$ = 1.9 K. Four-probe measurements, using the standard lock-in technique at 80.31 Hz, can be performed due to the reasonably good ohmic contacts. Figure 3a shows the four-terminal resistance $R_{13,24}$ as a function of the magnetic field $B$, at $n = 3.7 \times 10^{12}$ cm$^{-2}$. We observe SdHO starting at $B \approx 0.9$ T, which yields a lower boundary for the quantum mobility of about 11 000 cm$^2$/(V s), which is in agreement with the measured van der Pauw mobility of 7000 cm$^2$/(V s). Figure 3b displays four-terminal resistance $\Delta R_{13,24}$ with a smooth background subtracted, as a function of $B$, at $n = 5.2 \times 10^{12}$ cm$^{-2}$. Distinctive features appear above $B \approx 4$ T on top of the SdHO. They first emerge as shoulder-like features developing then into local minima in the SdHO as shown in Figure 3b with red arrows. From the

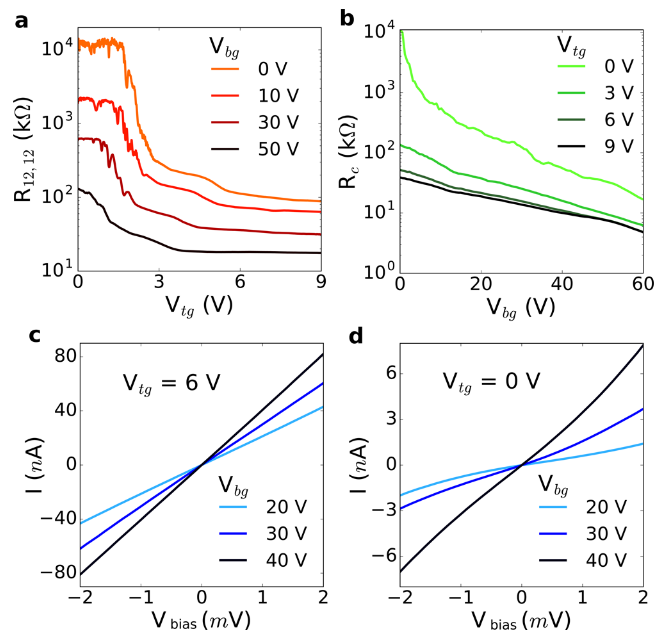


**Figure 2.** (a) Two-terminal resistance as a function of $V_{tg}$ at different $V_{bg}$, $R_{12,12}$, refers to contact numbering in Figure 1b, $T$ = 4 K. The resistance decreases by up to 2 orders of magnitude by biasing the gates on top of the contact area between graphene and $MoS_2$. The effect of the top gates decreases with increasing $V_{bg}$ due to the flattening of the $MoS_2$ conduction band at the interface. The resistances stop decreasing above $V_{tg}$ = 5 V, where the $MoS_2$ sheet resistance and the residual contact resistance between $MoS_2$ and graphene persist. (b) Contact resistance as a function of $V_{bg}$ at different $V_{tg}$. Biasing the top gates decreases the contact resistance by up to 3 orders of magnitude. (c) Linear $I$ $V_{bias}$ behavior is observed when $V_{tg} > 3$ V. (d) With $V_{tg}$ = 0 V, nonlinear $I-V_{bias}$ behavior is observed.

SdHO, we can determine the density of the 2DEG, $n = (de/h)(1/\Delta(1/B))$ where $\Delta(1/B)$ is the period of the SdHO and the prefactor $d$ accounts for spin and valley degeneracies. The electron density calculated from SdHO matches the Hall density when $d$ = 6. As shown in Figure 3b, a 6-fold LL degeneracy is clearly observed at relatively low magnetic field. Above 4 T additional minima for filling factors $\nu$ = 27, 33, 39, and 45 appear. The degeneracy of 6 arises from the 3 Q and 3 Q′ valleys located along $\Gamma-K$ symmetry lines in the first Brillouin zone (inset of Figure 3b), which correspond to the 6 degenerate conduction band minima expected from the band structure calculations of trilayer $MoS_2$.[12,22−26] The spin degeneracy within each Q and Q′ valley is already lifted by broken inversion and time reversal symmetry. At relatively high magnetic fields, due to the opposite spin character at Q and Q′ valley in 2D TMDC[26,27] the Zeeman splitting becomes comparable to the LL splitting and we observe the LL sextet being lifted into two LL triplets (inset of Figure 3b). Figure 3c shows $\Delta R_{13,24}$ as a function of the magnetic field component perpendicular to the 2DEG plane ($B_\perp$) at different angles $\theta$ (inset of Figure 3c). The SdHOs remain unchanged for all values of $\theta$ up to $\theta = 70°$. A similar behavior was observed for mono- and bilayer $WSe_2$.[28] The insensitivity of the Zeeman energy to the parallel component of the magnetic field may indicate that the electron spin is locked perpendicular to the plane due to the strong spin−orbit coupling and broken inversion symmetry in trilayer $MoS_2$.[12]


DOI: 10.1021/acs.nanolett.7b02186
Nano Lett. 2017, 17, 5008−5011

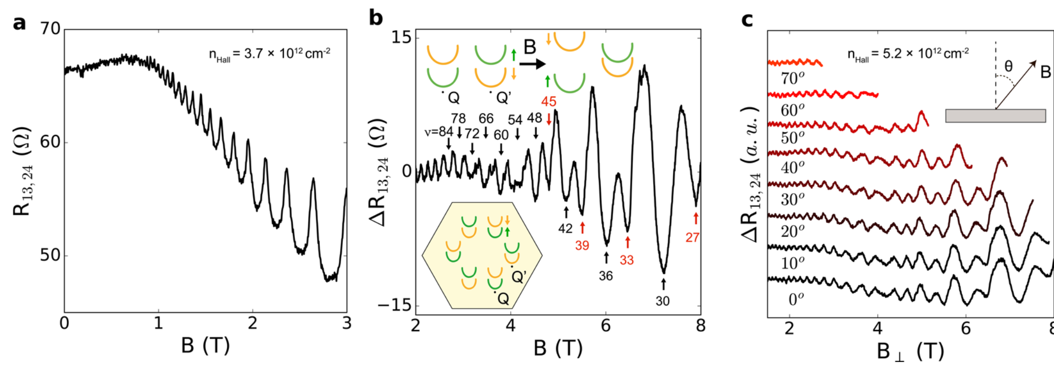

Figure 3. (a) Four-terminal resistance as a function of B field for a 3L $MoS_2$ device measured at $T$ = 1.9 K; $n = 3.7 \times 10^{12}$ $cm^{-2}$. (b) Background subtracted four-terminal resistance as a function of $B$ field at $n = 5.2 \times 10^{12}$ $cm^{-2}$. The LL filling factors are labeled for the oscillation minima. The degeneracy of 6 arises from the degeneracy of the 3 Q and 3 Q′ valleys in the conduction band (black arrows). Because of time reversal symmetry at $B$ = 0 T and broken inversion symmetry, the spin degeneracy within each Q or Q′ valley is already lifted. The degeneracy of 6 can be lifted at relatively high magnetic field due to the valley Zeeman effect (red arrows). Insets: Schematic diagrams for the Bloch bands of 3L $MoS_2$. When $B$ = 0 T, Q and Q′ valleys are degenerate, spin up is displayed in green, spin down in orange. When $B$ > 0 T, the valley Zeeman effect lifts the degeneracy. (c) SdHO shown in (b) as a function of $B_\perp$ at different tilted angles. The traces are shifted vertically for clarity. Inset: schematic of the sample orientation with respect to the magnetic field $B$.

High-quality $MoS_2$ 2DEGs allow us to investigate quantum transport in gate-defined nanostructures. As shown in the inset of Figure 4a, we define a constriction, 100 nm wide and 200 nm long, by electrostatically depleting the $MoS_2$ layer. In Figure 4a, we display the measured four-terminal conductance $G_{12,34}$ in unit of the conductance quantum,[29,30] $e^2/h$, as a function of $V_{sg}$ and $V_{bg}$, at $T$ = 1.9 K. At higher electron density, that is, higher $V_{bg}$, a more negative $V_{sg}$ is required in order to pinch off the $MoS_2$ channel with on−off ratios exceeding $10^5$. Figure 4b shows $G_{12,34}$, close to pinch-off at different $V_{bg}$. At relatively high carrier density ($n \approx 5 \times 10^{12}$ $cm^{-2}$, Figure 4b), we observe a significant decrease of resonances close to pinch-off, which we attribute to localized states forming in the electrostatically confined channel. These states, caused by the disorder potential in the $MoS_2$, may be better screened at high carrier density. At $B$ = 0 T, we observe even-spaced plateau-like features within 2 and 5 $e^2/h$. While plateau-like features are expected at multiples of 6 $e^2/h$, the experimental results show features that are roughly spaced by $e^2/h$, and even these values are not met precisely. Level degeneracies might be lifted by the additional confinement of the quantum point contact. However, we do not know the exact reason why the experimental data show plateau-like features that match only qualitatively a quantization with values around multiples of $e^2/h$. Further improvement of the 2DEG quality is required to demonstrate exact conductance quantization. Figure 4b shows raw data for the conductance. Subtracting a series resistance to account for possible contributions of the surrounding areas of the electron gas did not lead to a better matching of the plateau-like features with the expected values of the conductance quantization.

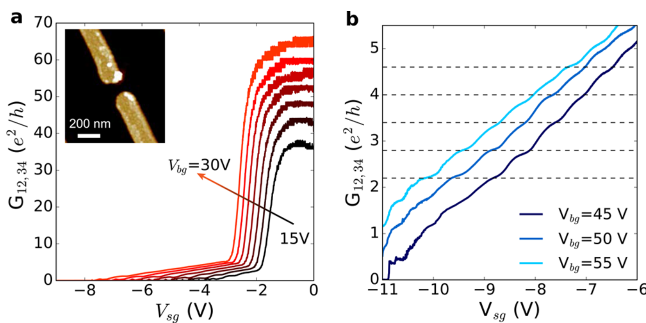

Figure 4. (a) Evolution of four-terminal conductance pinch off curves as a function of $V_{bg}$ at $T$ = 1.9 K. The QPC channel can be pinched off over a large range of electron density. Inset: AFM micrograph of the QPC split gate. The opening is 100 nm wide and 200 nm long. (b) Four-terminal conductance as a function of $V_{sg}$ at various $V_{bg}$. Plateau-like features, marked by horizontal dashed lines, appear with a spacing compatible with $e^2/h$.

**Conclusion.** In conclusion, we have developed a van der Waals heterostructure platform that allows us to obtain high-quality 2DEGs in $MoS_2$, displaying an electron mobility of 7000 $cm^2/(V\ s)$ with electron density as low as $\sim 10^{12}$ $cm^{-2}$. We observe SdHO starting at magnetic fields as low as 0.9 T with a 6-fold LL degeneracy that is lifted into a 3-fold LL with magnetic field. We further observe signatures of quantized conductance by electrostatically depleting a split gate on the $MoS_2$ 2DEG. The realization of an electrostatically tunable tunneling barrier reaching full pinch-off is the first step toward gate-defined quantum dots in 2D semiconducting TMDC in order to control and manipulate the spin and valley states of single confined electrons.[2,31,32]

During preparation of the manuscript, we became aware of related works.[6,33]

## AUTHOR INFORMATION


### Corresponding Author

*E-mail: pisonir@phys.ethz.ch.

### ORCID

Riccardo Pisoni: 0000-0003-1609-2846

Hiske Overweg: 0000-0002-9107-4763


### Notes

The authors declare no competing financial interest.

## ACKNOWLEDGMENTS

We thank Guido Burkard, Andras Kis, Matija Karalic, and Christopher Mittag for fruitful discussions. We acknowledge financial support by the Graphene Flagship, the EU Spin-Nano RTN network, and by the National Center of Competence in Research on Quantum Science and Technology (NCCR QSIT) funded by the Swiss National Science Foundation. Growth of hexagonal boron nitride crystals was supported by the

Elemental Strategy Initiative conducted by the MEXT, Japan and JSPS KAKENHI Grant Numbers JP15K21722.

## ■ REFERENCES


(1) Hanson, R.; Kouwenhoven, L. P.; Petta, J. R.; Tarucha, S.; Vandersypen, L. M. K. Spins in few-electron quantum dots. *Rev. Mod. Phys.* **2007**, *79*, 1217−1265.

(2) Loss, D.; DiVincenzo, D. P. Quantum computation with quantum dots. *Phys. Rev. A: At., Mol., Opt. Phys.* **1998**, *57*, 120−126.

(3) Petta, J. R.; Johnson, A. C.; Taylor, J. M.; Laird, E. A.; Yacoby, A.; Lukin, M. D.; Marcus, C. M.; Hanson, M. P.; Gossard, A. C. Coherent Manipulation of Coupled Electron Spins in Semiconductor Quantum Dots. *Science* **2005**, *309*, 2180−2184.

(4) Goossens, A. S. M.; Driessen, S. C. M.; Baart, T. A.; Watanabe, K.; Taniguchi, T.; Vandersypen, L. M. K. Gate-Defined Confinement in Bilayer Graphene-Hexagonal Boron Nitride Hybrid Devices. *Nano Lett.* **2012**, *12*, 4656−4660.

(5) Song, X.-X.; Liu, D.; Mosallanejad, V.; You, J.; Han, T.-Y.; Chen, D.-T.; Li, H.-O.; Cao, G.; Xiao, M.; Guo, G.-C.; et al. A gate defined quantum dot on the two-dimensional transition metal dichalcogenide semiconductor WSe2. *Nanoscale* **2015**, *7*, 16867−16873.

(6) Wang, K.; Taniguchi, T.; Watanabe, K.; Kim, P. Engineering Quantum Confinement in Semiconducting van der Waals Heterostructure. 2016, arXiv:1610.02929, accessed January 2017.

(7) Novoselov, K. S.; Jiang, D.; Schedin, F.; Booth, T. J.; Khotkevich, V. V.; Morozov, S. V.; Geim, A. K. Two-dimensional atomic crystals. *Proc. Natl. Acad. Sci. U. S. A.* **2005**, *102*, 10451−10453.

(8) Li, Y.; Ludwig, J.; Low, T.; Chernikov, A.; Cui, X.; Arefe, G.; Kim, Y. D.; van der Zande, A. M.; Rigosi, A.; Hill, H. M.; et al. Valley Splitting and Polarization by the Zeeman Effect in Monolayer MoSe2. *Phys. Rev. Lett.* **2014**, *113*, 266804.

(9) Srivastava, A.; Sidler, M.; Allain, A. V.; Lembke, D. S.; Kis, A.; Imamoğlu, A. Valley Zeeman effect in elementary optical excitations of monolayer WSe2. *Nat. Phys.* **2015**, *11*, 141−147.

(10) MacNeill, D.; Heikes, C.; Mak, K. F.; Anderson, Z.; Kormányos, A.; Zólyomi, V.; Park, J.; Ralph, D. C. Breaking of Valley Degeneracy by Magnetic Field in Monolayer MoSe2. *Phys. Rev. Lett.* **2015**, *114*, 037401.

(11) Aivazian, G.; Gong, Z.; Jones, A. M.; Chu, R.-L.; Yan, J.; Mandrus, D. G.; Zhang, C.; Cobden, D.; Yao, W.; Xu, X. Magnetic control of valley pseudospin in monolayer WSe2. *Nat. Phys.* **2015**, *11*, 148−152.

(12) Wu, Z.; Xu, S.; Lu, H.; Khamoshi, A.; Liu, G.-B.; Han, T.; Wu, Y.; Lin, J.; Long, G.; He, Y.; et al. Even−odd layer-dependent magnetotransport of high-mobility Q-valley electrons in transition metal disulfides. *Nat. Commun.* **2016**, *7*, 12955.

(13) Lee, G.-H.; Cui, X.; Kim, Y. D.; Arefe, G.; Zhang, X.; Lee, C.-H.; Ye, F.; Watanabe, K.; Taniguchi, T.; Kim, P.; et al. Highly Stable, Dual-Gated MoS2 Transistors Encapsulated by Hexagonal Boron Nitride with Gate-Controllable Contact, Resistance, and Threshold Voltage. *ACS Nano* **2015**, *9*, 7019−7026.

(14) Cui, X.; Lee, G.-H.; Kim, Y. D.; Arefe, G.; Huang, P. Y.; Lee, C.-H.; Chenet, D. A.; Zhang, X.; Wang, L.; Ye, F.; et al. Multi-terminal transport measurements of MoS2 using a van der Waals heterostructure device platform. *Nat. Nanotechnol.* **2015**, *10*, 534−540.

(15) Liu, Y.; Wu, H.; Cheng, H.-C.; Yang, S.; Zhu, E.; He, Q.; Ding, M.; Li, D.; Guo, J.; Weiss, N. O.; et al. Toward Barrier Free Contact to Molybdenum Disulfide Using Graphene Electrodes. *Nano Lett.* **2015**, *15*, 3030−3034.

(16) Xue, J.; Sanchez-Yamagishi, J.; Bulmash, D.; Jacquod, P.; Deshpande, A.; Watanabe, K.; Taniguchi, T.; Jarillo-Herrero, P.; LeRoy, B. J. Scanning tunnelling microscopy and spectroscopy of ultra-flat graphene on hexagonal boron nitride. *Nat. Mater.* **2011**, *10*, 282−285.

(17) Wang, L.; Meric, I.; Huang, P. Y.; Gao, Q.; Gao, Y.; Tran, H.; Taniguchi, T.; Watanabe, K.; Campos, L. M.; Muller, D. A.; et al. One-Dimensional Electrical Contact to a Two-Dimensional Material. *Science* **2013**, *342*, 614−617.

(18) Wang, J. I.-J.; Yang, Y.; Chen, Y.-A.; Watanabe, K.; Taniguchi, T.; Churchill, H. O. H.; Jarillo-Herrero, P. Electronic Transport of Encapsulated Graphene and WSe2 Devices Fabricated by Pick-up of Prepatterned hBN. *Nano Lett.* **2015**, *15*, 1898−1903.

(19) Zomer, P. J.; Guimarães, M. H. D.; Brant, J. C.; Tombros, N.; van Wees, B. J. Fast pick up technique for high quality heterostructures of bilayer graphene and hexagonal boron nitride. *Appl. Phys. Lett.* **2014**, *105*, 013101.

(20) Bretheau, L.; Wang, J. I.-J.; Pisoni, R.; Watanabe, K.; Taniguchi, T.; Jarillo-Herrero, P. Tunnelling spectroscopy of Andreev states in graphene. *Nat. Phys.* **2017**, DOI: 10.1038/nphys4110.

(21) Cao, Y.; Mishchenko, A.; Yu, G. L.; Khestanova, E.; Rooney, A. P.; Prestat, E.; Kretinin, A. V.; Blake, P.; Shalom, M. B.; Woods, C.; et al. Quality Heterostructures from Two-Dimensional Crystals Unstable in Air by Their Assembly in Inert Atmosphere. *Nano Lett.* **2015**, *15*, 4914−4921.

(22) Cheiwchanchamnangij, T.; Lambrecht, W. R. L. Quasiparticle band structure calculation of monolayer, bilayer, and bulk MoS2. *Phys. Rev. B: Condens. Matter Mater. Phys.* **2012**, *85*, 205302.

(23) Wang, Q. H.; Kalantar-Zadeh, K.; Kis, A.; Coleman, J. N.; Strano, M. S. Electronics and optoelectronics of two-dimensional transition metal dichalcogenides. *Nat. Nanotechnol.* **2012**, *7*, 699−712.

(24) Mak, K. F.; Lee, C.; Hone, J.; Shan, J.; Heinz, T. F. Atomically Thin MoS2: A New Direct-Gap Semiconductor. *Phys. Rev. Lett.* **2010**, *105*, 136805.

(25) Cappelluti, E.; Roldán, R.; Silva-Guillén, J. A.; Ordejón, P.; Guinea, F. Tight-binding model and direct-gap/indirect-gap transition in single-layer and multilayer MoS2. *Phys. Rev. B: Condens. Matter Mater. Phys.* **2013**, *88*, 075409.

(26) Chhowalla, M.; Shin, H. S.; Eda, G.; Li, L.-J.; Loh, K. P.; Zhang, H. The chemistry of two-dimensional layered transition metal dichalcogenide nanosheets. *Nat. Chem.* **2013**, *5*, 263−275.

(27) Xiao, D.; Liu, G.-B.; Feng, W.; Xu, X.; Yao, W. Coupled Spin and Valley Physics in Monolayers of MoS2 and Other Group-VI Dichalcogenides. *Phys. Rev. Lett.* **2012**, *108*, 196802.

(28) Movva, H. C. P.; Fallahazad, B.; Kim, K.; Larentis, S.; Taniguchi, T.; Watanabe, K.; Banerjee, S. K.; Tutuc, E. Density-Dependent Quantum Hall States and Zeeman Splitting in Monolayer and Bilayer $WSe_2$. 2017, arXiv:1702.05166, accessed March 2017.

(29) Wharam, D. A.; Thornton, T. J.; Newbury, R.; Pepper, M.; Ahmed, H.; Frost, J. E. F.; Hasko, D. G.; Peacock, D. C.; Ritchie, D. A.; Jones, G. A. C. One-dimensional transport and the quantisation of the ballistic resistance. *J. Phys. C: Solid State Phys.* **1988**, *21*, L209.

(30) van Wees, B. J.; van Houten, H.; Beenakker, C. W. J.; Williamson, J. G.; Kouwenhoven, L. P.; van der Marel, D.; Foxon, C. T. Quantized conductance of point contacts in a two-dimensional electron gas. *Phys. Rev. Lett.* **1988**, *60*, 848−850.

(31) Novoselov, K. S.; Mishchenko, A.; Carvalho, A.; Neto, A. H. C. 2D materials and van der Waals heterostructures. *Science* **2016**, *353*, aac9439.

(32) Kormányos, A.; Zólyomi, V.; Drummond, N. D.; Burkard, G. Spin-Orbit Coupling, Quantum Dots, and Qubits in Monolayer Transition Metal Dichalcogenides. *Phys. Rev. X* **2014**, *4*, 011034.

(33) Epping, A.; Banszerus, L.; Güttinger, J.; Krückeberg, L.; Watanabe, K.; Taniguchi, T.; Hassler, F.; Beschoten, B.; Stampfer, C. Quantum transport through $MoS_2$ constrictions defined by photodoping. 2016, arXiv:1612.01118, accessed January 2017.




DOI: 10.1021/acs.nanolett.7b02186
*Nano Lett.* 2017, 17, 5008−5011